A Speed-Constrained Sliding Mode Position Controller for PMLSM Based on Control Barrier Function

Zekun Wang, *Student Member, IEEE*, Chun He, Yong Li, Mingqiao Wang, *Member, IEEE*, and Chenxiao Jiu

***Abstract*—Sliding mode control (SMC) is widely used in the servo system of permanent magnet linear synchronous motor (PMLSM) and the problem of speed constraint exists in conventional sliding mode position controller (SMPC). The position speed integrated sliding mode controller (PSISMC) is an effective method to constrain speed for SMC due to its advantages of fast response and safety. However, the cascaded sliding mode surface structure of PSISMC makes the sliding mode surface design more complicated, and the low-speed crawling phenomenon in servo system of PMLSM may also affect the positioning accuracy. To handle these issues, a speed-constrained SMPC based on the control barrier function (CBF) is proposed in this article. By introducing CBF, the speed constraint is transformed into a constrained quadratic programming problem of q-axis current, achieving speed constraint while avoiding the use of cascaded sliding mode surfaces. A good speed constraining effect can be achieved by appropriately selecting the parameters of CBF. In addition, a new sliding mode reaching law consisting of the double power reaching law (DPRL) and a supertwisting-like integral term is proposed. Compared with the exponential reaching law in PSISMC, DPRL can alleviate the contradiction between sliding mode chattering and convergence speed. The supertwisting-like term is proposed and designed to alleviate the low-speed crawling phenomenon. Finally, experiments have demonstrated the advantages of CBF-SMC in positioning and tracking performance, as well as the effectiveness of its speed constraint capability.**

***Index Terms*—Control barrier function (CBF), permanent magnet linear synchronous motor (PMLSM), position servo system, sliding mode position controller (SMPC), speed constraint.**

I. Introduction

PERMANENT magnet linear synchronous motor (PMLSM) is widely used in high-performance servo systems [1] such as long-distance transportation [2], aerospace [3], computer numerical control machine tools [4] and medical field [5]. The field-oriented control (FOC) with P-PI cascaded structure is a typical control strategy for servo system of PMLSM due to its advantage such as simplicity and safety (easily constrained system state). However, the cascaded structure of FOC limits its dynamic response as well as accuracy [1], [6]. Furthermore, external disturbances exist in servo system of PMLSM such as parameter changes and friction forces also pose challenges to its servo control.

Several control methods have been proposed to meet these challenges, such as active disturbance rejection control (ADRC) [4], direct thrust control (DTC) [7], fuzzy control, model predictive control (MPC) [8] and sliding mode control (SMC) [9]. The ADRC method has the characteristics of weak coupling and strong robustness [10], and linear ADRC has become a standard paradigm for ADRC due to its stability being easy to prove and implementation being simple [11]. The DTC also received attention due to its insensitivity to motor parameters and simple design [7], [12]. In addition, the MPC method has been applied in permanent magnet synchronous motors (PMSMs) and power converters with a simple structure and system constraint [6], [13].

Recently, the SMC method has received widespread attention and has been applied in servo system of PMLSM due to its high response speed and insensitivity to parameter changes [14], [15]. The SMC method constructs a sliding mode surface based on the system reference input and system state. The system state reaches the sliding mode surface under the action of the sliding mode reaching law and converge along the sliding trajectory. Therefore, the design of sliding mode surface and reaching law are two key issues and main research contents of SMC. Linear sliding mode surface is used in traditional SMC, which has a simple design, but there is still room for optimization in its convergence speed. To accelerate the convergence, the terminal sliding mode control (TSMC) is proposed with a terminal sliding mode surface and it can achieve convergence in finite time [16]. However, TSMC method has singularity issues. The nonsingular terminal sliding mode control (NTSMC) is proposed to solve the problem of singularity [17]. In [18], a hierarchical NTSMC method is proposed for the speed regulation system of PMSM. The proposed NTSMC method combines the PID linear sliding mode control and NTSMC which can achieve convergence in finite time and exhibit faster convergence speed. In [19], a prescribed-time recursive NTSMC is proposed, this method

Received 11 August 2025; revised 18 October 2025; accepted 18 November 2025. Date of publication 25 November 2025; date of current version 25 February 2026. This work was supported by the Open Fund Project of Key Laboratory of Electric Drives & Propulsion Technology, Ministry of Education (Harbin Institute of Technology) under Grant BSAUEA5780200525. Recommended for publication by Associate Editor G. Scelba. *(Corresponding author: Chun He.)*

Zekun Wang, Chun He, Yong Li, and Mingqiao Wang are with the School of Electrical Engineering and Automation, Harbin Institute of Technology, Harbin 150001, China (e-mail: 22b906035@stu.hit.edu.cn; hit_hechun@hit.edu.cn; liyong611@hit.edu.cn; wangmingqiao@hit.edu.cn).

Chenxiao Jiu is with Xi'an Flight Automatic Control Research Institute, Xi'an 710065, China (e-mail: jiucx@avic.com).

Color versions of one or more figures in this article are available at https://doi.org/10.1109/TPEL.2025.3637051.

Digital Object Identifier 10.1109/TPEL.2025.3637051

is simple and intuitive, allowing for the direct definition of convergence time while eliminating singularity, regardless of the initial conditions and parameters of the system.

The sliding mode reaching law also has a significant impact on the performance of SMC, especially in terms of sliding mode chattering and convergence speed. Some studies are dedicated to improve the performance of sliding mode reaching laws. In [7], a new sliding mode reaching law is proposed for DTC of linear metro. The double power reaching law (DPRL) is combined with DTC and compared with the traditional exponential reaching law (ERL), the proposed DPRL has a faster convergence speed and smaller chattering phenomenon. The DPRL-DTC also exhibits stronger robustness and higher tracking accuracy. In [20], a new compound reaching law (NCRL) is proposed for the speed control of PMSM. The NCRL combines the exponential function and the power term piecewise function. Its arrival time is independent of the system state and alleviates the contradiction between convergence speed and sliding mode chattering. In [21], a new variable rate reaching law is proposed. The convergence time of the new reaching law is independent of system state, and can improve robustness while reducing sliding mode chattering. In addition, high-order sliding mode control not only retains the robustness of SMC, but also helps to solve the problem of sliding mode chattering [22]. In [1], the supertwisting sliding mode control (STSMC) is combined with NTSMC. A new nonsingular sliding mode surface is proposed for STSMC, which combines the characteristics of nonsingular terminal sliding mode surface and linear sliding mode surface. In [23], a new supertwisting-like fractional controller (STLFC) is proposed. The STLFC replaces the sign function in the integral term with a smooth function, significantly reducing sliding mode chattering.

A general sliding mode position controller (SMPC) has a position-speed loop integrated structure, and its speed cannot be directly constrained like FOC. The trajectory planning method can achieve SMC while constrain speed and has achieved good results [24]. However, trajectory planning method may limit the flexibility of its application. The position speed integrated sliding mode controller (PSISMC) does not require trajectory planning and achieves speed constraint by constructing the position speed cascade sliding mode surface [25]. However, the cascaded sliding mode surface structure of PSISMC limits the flexibility of sliding mode surface design, and there is also room for improvement in the reaching law performance. Some position control algorithms based on optimal control use external functions to achieve speed constraint, such as [6], the combination of long prediction horizon PPC and Laguerre function simultaneously achieves constraint on current, speed and voltage. Finally, the concept of control barrier function (CBF) is proposed in [26]. The CBFs are unified with control Lyapunov functions via quadratic programming (QP). This allows the system to achieve control objectives under constrained conditions. Shao et al. [27] provides a detailed review of the combination of CBF and SMC, providing a reference for predefined methods of SMC performance. In [28], CBF successfully combined with SMC. The proposed Barrier function-based adaptive sliding mode method takes into account actuator saturation and the uncertainty of nonlinear systems, enabling the tracking error of the system to converge within a predefined range. In [29], the use of CBF in motor systems effectively improves the performance of sensorless control methods for motors. In summary, these research findings provide new ideas for the speed constraint in position-speed loop integrated control structure like SMPC.

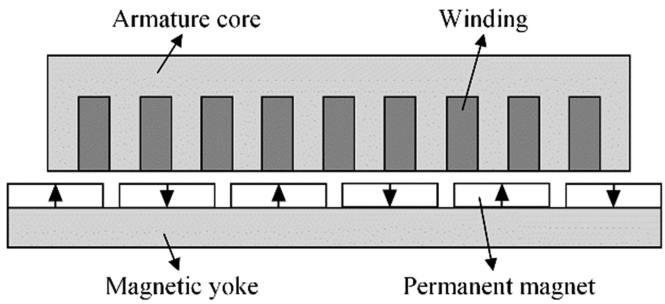

Fig. 1. Structure of PMLSM.

Motivated by the above discussion, the main contributions of this article are summarized as follows:

1) A new speed constraint method for SMPC of PMLSM is proposed in this article. CBF and SMPC are integrated for speed constraint, which avoids the use of cascaded sliding mode surfaces and enhances the flexibility of speed constraint.
2) A new sliding mode reaching law for CBF-SMC is proposed, which can alleviate the contradiction between sliding mode chattering and convergence speed while effectively suppressing the low-speed crawling phenomenon in the position control system of PMLSM.
3) The stability of the proposed CBF-SMC method is analyzed. Comparative experimental tests are organized, which demonstrates the effectiveness of speed constraint as well as the superiority in tracking performance and positioning performance of CBF-SMC.

II. Conventional Position Speed Integrated Sliding Mode Controller

A. Mechanical Model of PMLSM

The structure of PMLSM in this article can be divided into the mover (primary) and the stator (secondary). The mover is composed of the armature core and three-phase windings. After energizing the mover winding, a traveling wave magnetic field is generated to drive the mover. The stator is composed of the magnetic yoke and permanent magnets. For the surface-mounted PMLSM in this article, the permanent magnets are evenly distributed on the magnetic yoke. Fig. 1 shows the structure of PMLSM.

Under the d–q synchronous rotating frame, the d-axis leads the q-axis by $\frac{\pi}{2}$ rad electrical angle and the thrust equation of PMLSM can be expressed as

$$F_{\mathrm{e}} = \frac{3\pi}{2\tau} p_n i_q [\psi_f + (L_d - L_q) i_d] \tag{1}$$

where F_e is the is electromagnetic thrust. i_d and i_q are the d- and q-axis stator currents, respectively. L_d and L_q are the d- and

q-axis stator inductance, respectively. p_n is the pole pairs, τ is the pole pitch and ψ_f is the permanent-magnet flux linkage.

For the surface-mounted PMLSM in this article, $L_d = L_q$ and (1) can be rewritten as

$$F_e = \frac{3\pi}{2\tau} p_n \psi_f i_q = k_f i_q \tag{2}$$

where $k_f = \frac{3\pi}{2\tau}\, p_n \psi_f$ is the thrust coefficient.

Considering disturbances, the mechanical equation of PMLSM can be expressed as

$$\begin{cases} \dot{x} = v \\ \dot{v} = -\frac{B_0}{M_0} v + \frac{k_{f0}}{M_0} i_q - \frac{F_d}{M_0} \end{cases} \tag{3}$$

where x is the position of the mover. v is the speed of the mover. M_0 is the nominal value of the mover mass. B_0 is the nominal value of the viscous friction coefficient. k_{f0} is the nominal value of the thrust coefficient. F_d is the total disturbance force and it can be expressed as

$$F_d = -\Delta k_f i_q + \Delta M \dot{v} - \Delta B v + F_{\text{fric}} + F_r + F_{\text{ext}} + \varepsilon_F \tag{4}$$

where $\Delta M = M - M_0$ is the change value of the mover mass. $\Delta B = B - B_0$ is the change value of the viscous friction coefficient. $\Delta k_f = k_f - k_{f0}$ is the change value of the thrust coefficient. F_{fric} is the friction force. F_r is the detent force. F_{ext} is the external disturbance force including cable drag force and load force. ε_F is other unmodeled disturbance force, such as the disturbance caused by the nonlinear characteristics of the inverter.

To simplify analysis, the mechanical equation of PMLSM in (3) can be rewritten as

$$\begin{cases} \dot{x} = v \\ \dot{v} = m_0 i_q + f_d \end{cases} \tag{5}$$

where $m = \frac{k_f}{M}$, m_0 is the nominal value of m and $f_d = -\frac{B_0 v + F_d}{M_0}$.

B. Conventional PSISMC

Conventional PSISMC achieves speed constraint in the position-speed loop integrated structure by constructing cascaded sliding mode surfaces [25], which can be expressed as

$$\begin{cases} s_1 = c(x^* - x) + (v^* - v) \\ \dot{s}_1 = -\varepsilon \text{sign}(s) - qs \end{cases} \tag{6}$$

$$\begin{cases} s_2 = (v^* - v) + v_{\max} \\ \dot{s}_2 = -\varepsilon \text{sign}(s) - qs \end{cases} \tag{7}$$

where x^* is the reference position. $v^* = \dot{x}^*$ is the reference speed. $v_{\max}$ is the maximum value of v. c, ε, and q are all positive constants.

Fig. 2 shows two working modes of PSISMC. When $v_{\max}$ is large or x^* is close to x, PSISMC adopts sliding mode surface s_1 for position control. When $v_{\max}$ is small or x^* is far, v will reach $v_{\max}$ under position control. At this point, PSISMC will switch to sliding mode surface s_2 to maintain maximum speed, and switch back to s_1 when mover approaches x^* to ensure smooth arrival.

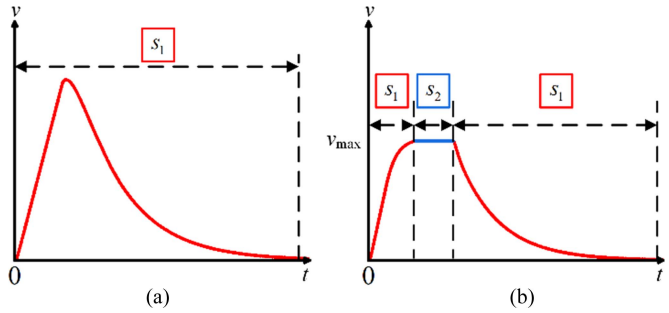

Fig. 2. Speed trajectory of PSISMC in different operating modes. (a) Position control only. (b) Integrated position and speed control.

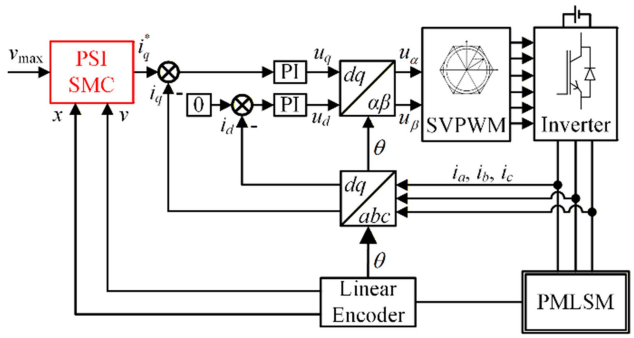

Fig. 3. Block diagram of conventional PSISMC.

Fig. 3 illustrates the block diagram of conventional PSISMC.

Remark 1: According to (6) and (7), there is room for improvement in the sliding mode reaching law of conventional PSISMC. The constant term $\varepsilon \text{sign}(s)$ in the ERL may produce oscillations when the mover approaches the reference position, which may have an adverse effect on the accuracy of position control. This can be improved by replacing it with a smooth function.

Remark 2: Compared with PMSM, PMLSM exhibits low-speed crawling of the mover due to the interference of sliding friction force. However, the conventional PSISMC resists external disturbances at the cost of steady-state error, which seriously affects the point-to-point positioning accuracy and limits its application in PMLSM.

III. Design of Sliding Mode Position Controller Based on Control Barrier Function

A. Design of SMC

The sliding mode surface of the proposed CBF-SMC is designed as

$$s = c(x^* - x) + (v^* - v) \tag{8}$$

where constant $c > 0$.

The sliding mode reaching law of CBF-SMC is designed as

$$\begin{aligned} \dot{s} &= -k_1 |s|^{\alpha} \text{sat}(s) - k_2 |s|^{1+\alpha} \text{sat}(s) - u_{st} \\ &= -u_{dp} - u_{st} \end{aligned} \tag{9}$$

$$u_{dp} = k_1|s|^{\alpha}\text{sat}(s) + k_2|s|^{1+\alpha}\text{sat}(s) \tag{10}$$

where parameters $k_1 > 0$, $k_2 > 0$ and $0 < \alpha < 1$. The integral term u_{st} will be designed later. sat$(\cdot)$ is the saturation function which can be expressed as

$$\text{sat}(s) = \begin{cases} 1, & s > \Delta \\ s/\Delta, & -\Delta \le s \le \Delta \\ -1, & s < -\Delta \end{cases} \tag{11}$$

where parameter $\Delta > 0$ is the boundary of the saturation function and sufficiently small.

Remark 3: Compared with conventional PSISMC, the proposed CBF-SMC adopts the DPRL to replace the original ERL. The original term $\varepsilon\text{sign}(s)$ is replaced with term $k_1|s|^{\alpha}\text{sign}(s)$ to better balance convergence speed and chattering, and when the system is far from the sliding trajectory, DPRL adopts term $k_2|s|^{1+\alpha}\text{sign}(s)$ to increase the convergence speed. The switching function sign$(\cdot)$ is replaced with the saturation function sat$(\cdot)$ to further weakening sliding mode chattering.

Combining (5), (8), (9), (10) and taking the derivative of s, the control law i_s of CBF-SMC can be expressed as

$$\begin{aligned} i_s &= \tfrac{1}{m_0}[c(v^* - v) - \dot{s}] \\ &= \tfrac{1}{m_0}[c(v^* - v) + u_{dp} + u_{st}]. \end{aligned} \tag{12}$$

B. Design of Control Barrier Function

Define the upper and lower limits of v are $v_{\max p}$ and $v_{\max n}$, respectively, i.e., $-v_{\max n} \le v \le v_{\max p}$.

Lemma 1 [26]: A closed set $\mathcal{C} \subset \mathbb{R}^n$ is defined as

$$\begin{cases} \mathcal{C} = \{x \in \mathbb{R}^n : h(x) \ge 0\} \\ \partial\mathcal{C} = \{x \in \mathbb{R}^n : h(x) = 0\} \\ \text{Int}(\mathcal{C}) = \{x \in \mathbb{R}^n : h(x) > 0\} \end{cases} \tag{13}$$

where Int(C) and ∂C denote the interior and boundary of the set C.

Consider the nonlinear affine control system

$$\dot{x} = f(x) + g(x)u \tag{14}$$

where $f(x) : \mathbb{R}^n \to \mathbb{R}^n$ and $g(x) : \mathbb{R}^n \to \mathbb{R}^n$ are locally Lipschitz, system state $x \in \mathbb{R}^n$ and control input $u \in \mathbb{R}$. Define a continuous function $\beta_1 : [0, a) \to [0, \infty)$ for some $a > 0$ belongs to class K if it is strictly increase and $\beta_1(0) = 0$, and the function $h(x)$ is a CBF on set C, if there exists a class K function τ_1 makes $h(x)$ satisfy the following condition:

$$\sup_{u \in U}\{L_f h(x) + L_g h(x)u + \tau_1(h(x))\} \ge 0 \tag{15}$$

where $L_f h(x) = \frac{\partial h(x)}{\partial x} f(x)$ and $L_g h(x) = \frac{\partial h(x)}{\partial x} g(x)$ are standard Lie derivatives. U is the constraint set of u.

Based on Lemma 1, define the safe speed set $\mathcal{C}_v = \{\text{v} \in \mathbb{R} : -\text{v}_{\max n} \le \text{v} \le \text{v}_{\max p}\}$, function $\bar{h}(v) = v_{\max p} - v$ and $\underline{h}(v) = v_{\max n} + v$. If there exists a positive constant τ_1 satisfy as

$$\sup_{i_q \in U}\{-m_o i_q\} \ge -\tau_1 \bar{h}(v) \tag{16}$$

$$\sup_{i_q \in U}\{m_o i_q\} \ge -\tau_1 \underline{h}(v) \tag{17}$$

then $\bar{h}(v)$ and $\underline{h}(v)$ are CBFs for servo system of PMLSM. $U = \{i_q \in \mathbb{R} : -i_{q\max} \le i_q \le i_{q\max}\}$ and $i_{q\max}$ is the amplitude limit of i_q.

Based on (16) and (17), the speed constraint of CBF-SMC can be regarded as a constrained QP problem described as follows:

$$\begin{aligned} i_q^* &= \underset{i_q \in U}{\text{argmin}} \tfrac{1}{2}\|i_q - i_s\|^2 \\ \text{s.t.} \quad & -\tau_1 \underline{h}(v) \le m_0 i_q \le \tau_1 \bar{h}(v). \end{aligned} \tag{18}$$

Assuming $|f_d| \le D_1$ and combining (5), (16) and (17), the actual i_q limit considering disturbance can be expressed as

$$-\tau_1\left(v_{\max n} + \frac{D_1}{\tau_1} + v\right) \le m_0 i_q \le \tau_1\left(v_{\max p} + \frac{D_1}{\tau_1} - v\right). \tag{19}$$

It can be concluded from (19) that the actual speed range will shift as shown in (20) without applying disturbance observer for compensation

$$-v_{\max n} - \frac{D_1}{\tau_1} \le v \le v_{\max p} + \frac{D_1}{\tau_1}. \tag{20}$$

Remark 4: It can be drawn from (19) and (20) that the larger τ_1, the stronger the antidisturbance performance of CBF, but the weaker the speed constraint capability, and vice versa. By appropriately selecting τ_1, CBF can achieve a compromise between speed constraint and antidisturbance performance. Compared with the speed constraint method of PSISMC, CBF-SMC uses one adjustable parameter of CBF to adjust the speed constraint while avoiding the complex control structure of two sliding mode surfaces, making the method more flexible to use.

In order to overcome the impact of low-speed crawling on positioning performance, this article designs the supertwisting-like integral term u_{st} that matches CBF-SMC and its discrete form can be expressed as

$$\begin{aligned} &u_{st}(k+1) \\ &= \begin{cases} u_{\text{pre}}, \\ \text{if } -\tau_1 \underline{h}(v) < m_0 i_q < \tau_1 \bar{h}(v) \text{ and } |u_{\text{pre}}| < u_{st\max} \\ u_{st\max}\text{sign}(u_{st}(k)), \\ \text{if } -\tau_1 \underline{h}(v) < m_0 i_q < \tau_1 \bar{h}(v) \text{ and } |u_{pre}| \ge u_{st\max} \\ 0, \\ \text{if } m_0 i_q \le -\tau_1 \underline{h}(v) \text{ or } m_0 i_q \ge \tau_1 \bar{h}(v) \end{cases} \end{aligned} \tag{21}$$

where $u_{\text{pre}} = u_{st}(k) + T_s k_3 \text{sat}(s)$ and T_s is the control period.

Remark 5: By designing (21), the u_{st} term only works when v has not reached the limit, which alleviates the low-speed crawling phenomenon while avoiding the desaturation process of the integral term, effectively improving the point-to-point positioning accuracy of CBF-SMC.

Remark 6: The speed constraint method based on CBF design in this article is similar in algorithm structure to MPC, and both use QP solvers for optimal control. However, the method in this article does not use long prediction horizon or matrix calculations, but instead uses purely numerical methods to calculate the current boundary corresponding to the speed constraint.

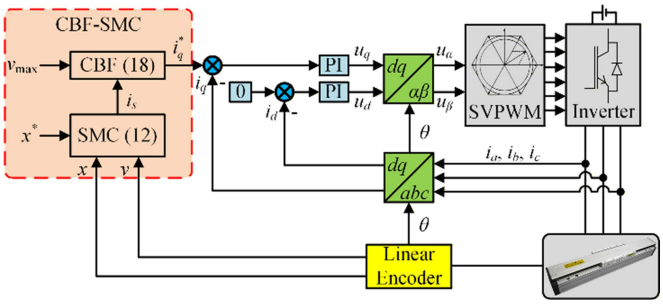

Fig. 4. Block diagram of CBF-SMC for PMLSM.

Therefore, the computational burden is tolerable and sufficient to run on a general control platform.

Fig. 4 illustrates the block diagram of CBF-SMC for servo system of PMLSM.

C. Stability and Performance Analysis of CBF-SMC

Referring to [22] and [30], the bounded input bounded output (BIBO) stability of the proposed CBF-SMC method is analyzed in this clause. The stability analysis can be constructed into two parts as follows. The convergence of position tracking error is proven in the first part. The speed constraint is always effective and is proven in the second part.

1) Part 1: According to (10), (12), and (18), when v has not reached the upper or lower constraint boundary and Δ is small enough, the control input i_q can be approximated as

$$i_q = \frac{1}{m_0}[c(v^* - v) + k_1|s|^{\alpha}\text{sign}(s) + k_2|s|^{1+\alpha}\text{sign}(s) + u_{st}]. \tag{22}$$

According to (5) and (22), considering disturbance f_d, it yields

$$\dot{s} = -k_1|s|^{\alpha}\text{sign}(s) - k_2|s|^{1+\alpha}\text{sign}(s) - u_{st} - f_d. \tag{23}$$

Define the *Lyapunov* function

$$V_1 = s^2/2. \tag{24}$$

The derivative of (24) can be expressed as

$$\begin{aligned}\dot{V}_1 &= s\dot{s} \\ &= -k_1|s|^{1+\alpha} - k_2|s|^{2+\alpha} - su_{st} - sf_d \\ &\le -k_1|s|^{1+\alpha} - k_2|s|^{2+\alpha} + D_2|s|\end{aligned} \tag{25}$$

where $D_2 = D_1 + u_{st\max}$. The sliding variable s and position error $\Delta x = x^* - x$ converge to the following bound

$$|s| \le \min\left\{\left(\frac{D_2}{k_1}\right)^{\frac{1}{\alpha}}, \left(\frac{D_2}{k_2}\right)^{\frac{1}{1+\alpha}}\right\} \tag{26}$$

$$|\Delta x| \le \min\left\{\frac{1}{c}\left(\frac{D_2}{k_1}\right)^{\frac{1}{\alpha}}, \frac{1}{c}\left(\frac{D_2}{k_2}\right)^{\frac{1}{1+\alpha}}\right\}. \tag{27}$$

2) Part 2: When the speed v reaches the upper constraint boundary, the control input i_q can be expressed as

$$i_q = \tau_1\bar{h}(v)/m_0. \tag{28}$$

Combing (5), (28) and define $s_v = v_{\max p} - v$, it can be obtained that

$$\dot{s}_v = -\tau_1 s_v - f_d. \tag{29}$$

Define the *Lyapunov* function

$$V_2 = s_v^2/2 \tag{30}$$

The derivative of (30) can be expressed as

$$\begin{aligned}\dot{V}_2 &= s_v\dot{s}_v \\ &= -\tau_1 s_v^2 - f_d s_v \\ &\le -\tau_1 s_v^2 + D_1|s_v|.\end{aligned} \tag{31}$$

According to (31), it can be concluded that at this point, the system satisfies the BIBO stability with the range of

$$|s_v| \le \frac{D_1}{\tau_1} \tag{32}$$

and speed v converges as (20) describes.

This completes the proof. For the case where v reaches the lower constraint boundary, the proof process is similar and will not be repeated here.

3) Performance Analysis: To analysis the chattering level of ERL in PSISMC method, it can be discretized as

$$s(t+1) - s(t) = -\varepsilon T_s\text{sign}(s(t)) - qT_s s(t). \tag{33}$$

When the system approaches the sliding mode surface and $s \to 0^+$, the range of movement of s is

$$s(t) = \varepsilon T_s. \tag{34}$$

With the decrease of s, when $s \to 0^-$, the range of movement of s is same as (34). The switching boundary of ERL in PSISMC can be expressed as

$$\Delta_1 = 2\varepsilon T_s. \tag{35}$$

For the reaching law in (9) of CBF-SMC, its chattering can be approximated as the superposition of u_{dp} and u_{st} terms. (10) can be discretized as

$$\begin{aligned}u_{dp}(t+1) - u_{dp}(t) = &-\frac{k_1}{\Delta}T_s|s(t)|^{\alpha+1}\text{sign}(s(t)) \\ &-\frac{k_2}{\Delta}T_s|s(t)|^{\alpha+2}\text{sign}(s(t)).\end{aligned} \tag{36}$$

Ignore high-order terms, the switching boundary of u_{dp} term can be expressed as

$$\Delta_{dp} = \frac{2k_1}{\Delta}T_s|s(t)|^{\alpha+1} = \frac{2k_1}{\Delta}T_s|c\Delta x(t)|^{\alpha+1} \tag{37}$$

where $\Delta x\ (t) = x^*\ (t) - x(t)$ is the discrete form of position error.

Comparing (35) and (37), it can be observed that u_{dp} avoids fixed switching boundaries and provides additional parameters Δ and α for adjusting sliding mode chattering. For the u_{st} term, the integral form makes its chattering relatively small. Therefore, it can be considered that the reaching law (9) has a smaller chattering level compared to ERL.

To verify the previous conclusion, simulate according to the parameters in Section IV and set the initial position error as 0.1,

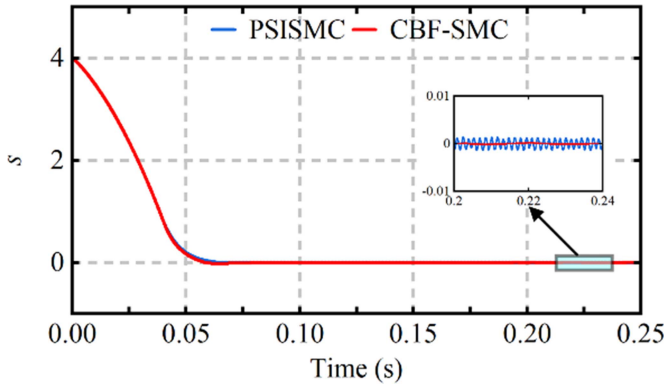

Fig. 5. Simulation of sliding trajectory of two methods.

which means the initial value of s is 4. The sliding trajectory of the system of two methods is shown in Fig. 5. It can be seen from this that the sliding variable s of both methods converges from 4 to 0, and the PSISMC method exhibits a larger chattering amplitude after convergence, which is consistent with previous theoretical analysis.

Similar to the calculation process in Part I, it is easy to determine the convergence range of position of PSISMC method when $\varepsilon \leq D_1$ as (38)

$$|\Delta x| \leq \frac{1}{c}\frac{D_1 - \varepsilon}{q} \tag{38}$$

when $\varepsilon > D_1$, Δx can converge to 0. However, when D_1 is large, according to (35), a larger ε will result in greater chattering. For CBF-SMC method, under the action of the integral term in (21), its steady-state position error can also converge to 0, thus achieving high positioning accuracy with smaller sliding mode chattering.

IV. Experiment Test Results

In this section, the positioning performance, tracking performance and speed constraint of the proposed CBF-SMC method is verified by comparison through experiment tests. The first method is the deadbeat predictive position control (DBPPC) in [31] with real-time feasibility, combined DBPPC with CBF in this article to achieve speed constraint. The second is the conventional PSISMC method. In addition, to further enhance the robustness of the method, the Luenberger observer in [31] is used as the disturbance observer in conjunction with the proposed method as the third method for testing.

The parameters of all the methods are listed as follows. Parameters of DBPPC method are $m = 20$, $\alpha = 0.9$, $\tau_1 = 500$, $\omega_o = 200$, and $m_0 = 18.04$, respectively. Parameters of PSISMC method are $c = 40$, $\varepsilon = 10$, $q = 120$, and $m_0 = 18.04$, respectively. Parameters of CBF-SMC are $c = 40$, $k_1 = 10$, $k_2 = 120$, $k_3 = 120$, $\alpha = 0.3$, $\Delta = 0.005$, $\tau_1 = 500$, and $m_0 = 18.04$, respectively. Parameters of CBF-SMC with DOB are $c = 40$ $k_1 = 10$, $k_2 = 120$, $k_3 = 120$, $\alpha = 0.3$, $\Delta = 0.005$, $\tau_1 = 500$, $m_0 = 18.04$, and $\omega_o = 200$, respectively. The integral saturation limit of CBF-SMC method is $u_{st} = 30$. The i_q saturation limit for all methods is $i_{q\max} = 2.5$.

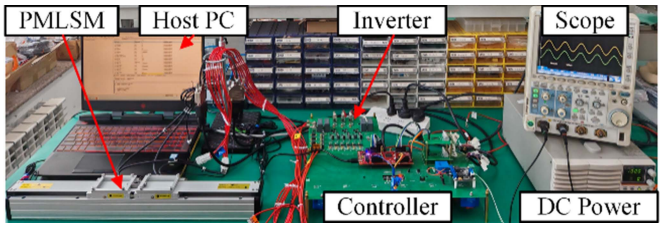

Fig. 6. Test bench.

TABLE I
Parameters of PMLSM

Symbol	Name	Value
τ	Pole pitch	0.01 m
L_d	d-axis inductance	14.1 mH
L_q	q-axis inductance	14.1 mH
R_s	Stator resistance	3.2 Ω
M	Mover mass	0.35 kg
ψ_f	Flux linkage	0.0268 Wb
p_n	Pole pairs	1
U_{DC}	DC-bus voltage	100 V

The experimental setup in Fig. 6 is used to test CBF-SMC. The LAUNCHXL-F28379D is used to execute the program, which is a DSP platform with 200 MHz frequency. A two-level voltage source inverter based on FS150R06KE3 is used to drive PMLSM and its parameters are given in Table I. A linear grating encoder with a resolution of 0.5 μm is used to measure the position signal. All methods are tested with 10 kHz frequency ($T_s = 100$ μs).

A. Positioning Performance Test

To verify the positioning performance of all methods, a step reference position signal with 0.1 at 0 s and 0 at 1s is applied to the system. $v_{\max p}$ and $v_{\max n}$ are both set as 2 m/s. The positioning performance of all methods are shown in Fig. 7.

According to Fig. 7, it can be seen that all methods reach the reference position rapidly. Fig. 7(a) shows the enlarged view of position from 0.98 to 0.99 s. The PSISMC method exhibits low-speed crawling phenomenon, which is manifested as the mover slowly approaching the reference position at a low speed after reaching the vicinity of the reference position, ultimately causing significant point-to-point positioning errors. This can also be seen from Fig. 7(c), where viscous friction force cause all methods to exhibit significant control signals around 1.0 s.

Define the position error as $\Delta x = x^* - x$ and the final $|\Delta x|$ under step reference signal is the static position error Δx_s. Δx_s of all methods are 0.0000340 m, 0.0027795 m, 0.0000195 m and 0.0000084 m, respectively. The proposed CBF-SMC method has the smallest Δx_s, which demonstrates that the method can effectively suppress low-speed crawling phenomenon and has significant advantages in positioning performance. DOB further reduces Δx_s of the CBF-SMC method, demonstrating the suppression effect of the DOB on external disturbances, such as friction.

In order to verify whether CBF-SMC would cause excessive computational burden, define the program execution cycle is Δt_c. All methods are tested with Δt_c of 21.5 μs, 21.0 μs, 25.4 μs,

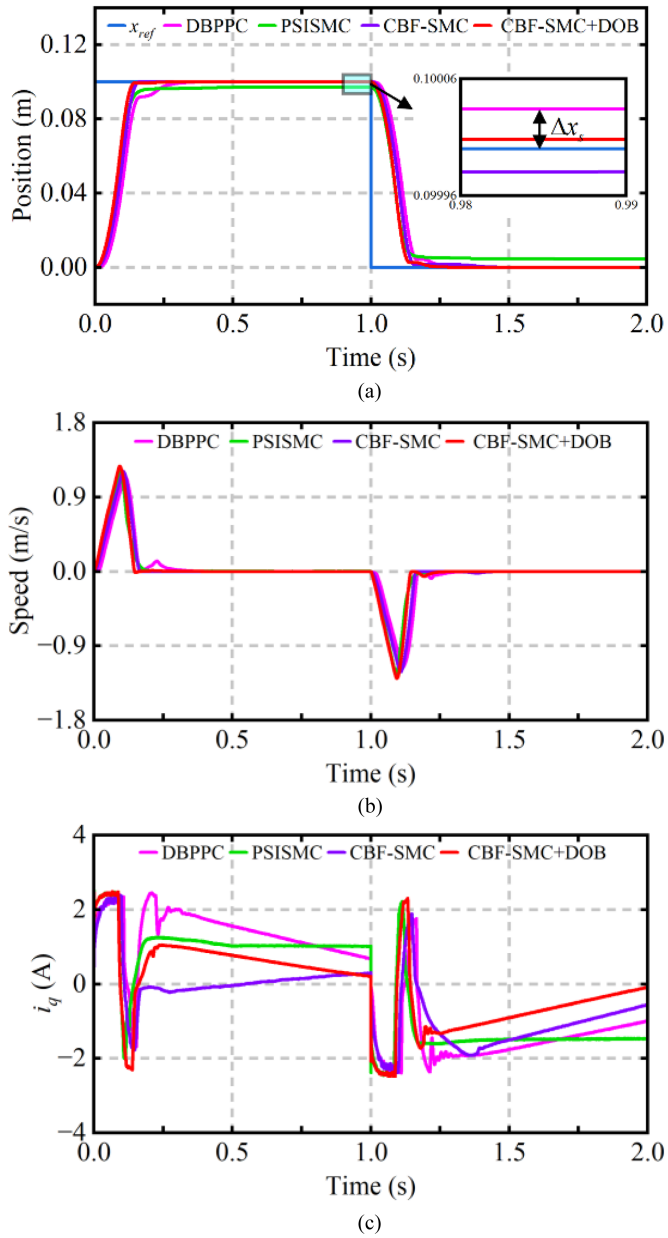

Fig. 7. Positioning performance under step reference position signal. (a) Position. (b) Speed. (c) q-axis current.

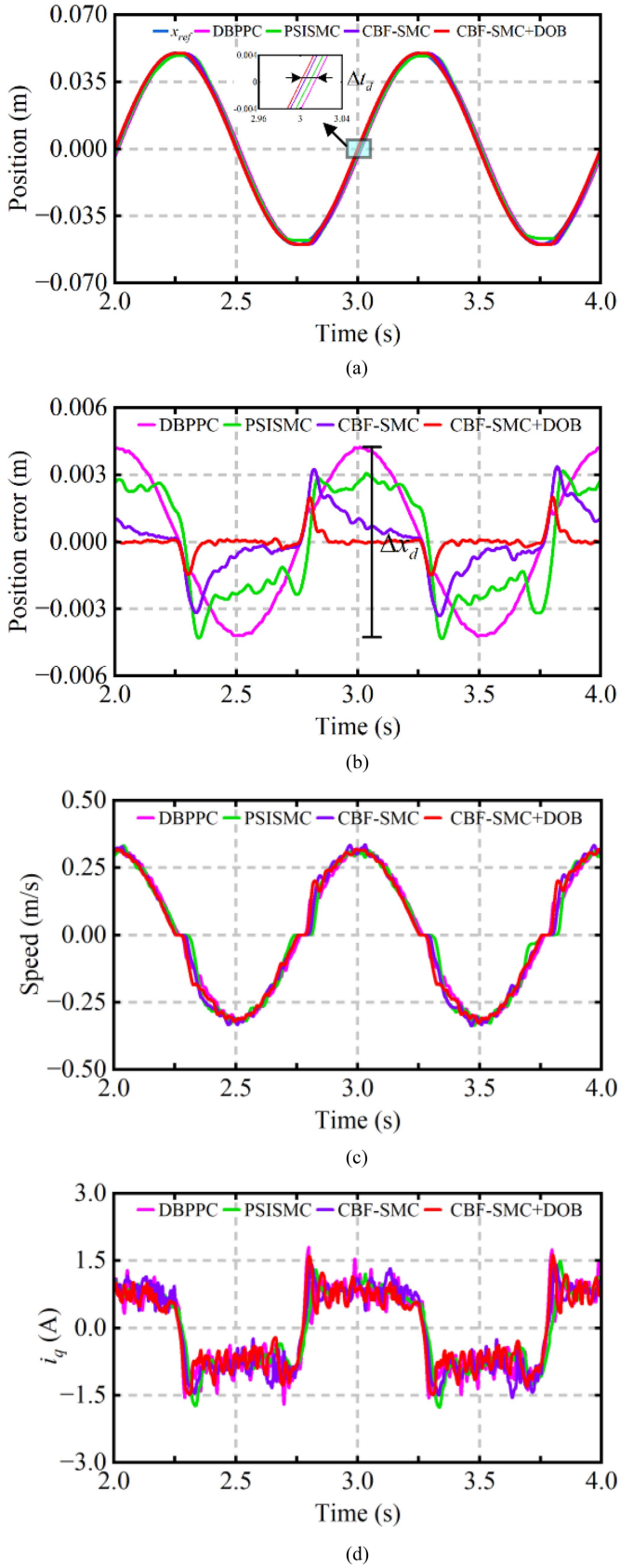

Fig. 8. Tracking performance under sine reference position signal. (a) Position. (b) Position error. (c) Speed. (d) q-axis current.

and 25.8 μs at $T_s = 100$ μs, respectively. This proves that the proposed method can run on the DSP platform without causing excessive computational burden.

B. Tracking Performance Test

Applying periodic reference position signals can effectively verify the position tracking performance of servo system. To verify the tracking performance of the proposed method, a sine reference position signal $x^* = 0.05\sin(2\pi t)$ is applied to the servo system of PMLSM. $v_{\max p}$ and $v_{\max n}$ are both set as 2 m/s. The tracking performance of all methods are shown in Fig. 8.

TABLE II
COMPARISON OF TRACKING AND POSITIONING PERFORMANCE

Items	Methods			
	DBPPC	PSISMC	CBF-SMC	CBF-SMC +DOB
Δx_s (m)	0.0000340	0.0027795	0.0000195	0.0000084
Δx_d (m)	0.0084566	0.0075005	0.0066746	0.0034938
Δt_d (s)	0.0135	0.0088	0.0035	0.0002
Δt_c (μs)	21.5	21.0	25.4	25.8

Fig. 8(a) shows the position response of all methods from 2 to 4 s, and it can be seen that all methods have well tracked the sine reference position signal. Define the position lag time as Δt_d. Δt_d of all methods under sine reference position are 0.0135 s, 0.0088 s, 0.0035 s, and 0.0002 s, respectively.

Fig. 8(b) shows the position error and Fig. 8(c) shows the speed response of all methods from 2 to 4 s. It can be seen that all methods experience crawling during the direction change of the sine reference signal due to the influence of friction, which has a negative impact on the dynamic position tracking performance of the servo system of PMLSM. This is also shown in Fig. 8(d) as the control signal, which should have been a small amplitude sine wave, but exhibits a larger amplitude. Define the peak-to-peak value of Δx under sine reference position signal is Δx_d. Δx_d of all methods under sine reference position are 0.0084566 m, 0.0075005 m, 0.0066746 m, and 0.0034938 m, respectively. From the above discussion, it can also be seen again that DOB compensates for external disturbances, such as slowing down the crawling phenomenon in Fig. 8(c). Finally, the positioning and tracking performance indicators of all methods are summarized and compared in Table II.

C. Speed Constraint Test

To verify the speed constraint capability of all methods, a step reference position signal with 0.1 at 0 s and 0 at 1s is applied to the system. $v_{\max p}$ and $v_{\max n}$ are both set as 0.8 m/s. The step response of all methods under speed constraint are shown in Fig. 9.

According to Fig. 9, it can be seen that under step reference position signal, the speed of all methods rapidly reaches and remains at 0.8 m/s. When approaching the reference position, speed rapidly drops to 0, allowing the mover to smoothly reach the reference position. The Δx_s of all methods under speed constraint are 0.0000201 m, 0.0029330 m, 0.0000160 m and 0.0000150 m, respectively. The results in Fig. 9 indicate that compared with the conventional PSISMC method, the proposed CBF-SMC method achieves higher point-to-point positioning accuracy while achieving speed constraint. It also confirms that the compensation effect of DOB is still effective under speed constraint.

To further validate the speed constraining capability of the CBF-SMC method, $v_{\max p}$ and $v_{\max n}$ are set to 0.8 m/s and 0.6 m/s, respectively. The step response of the CBF-SMC method under asymmetric speed constraint is shown in Fig. 10. The experimental results are consistent with the theory, proving that the proposed speed constraining method is still effective under asymmetric speed constraint.

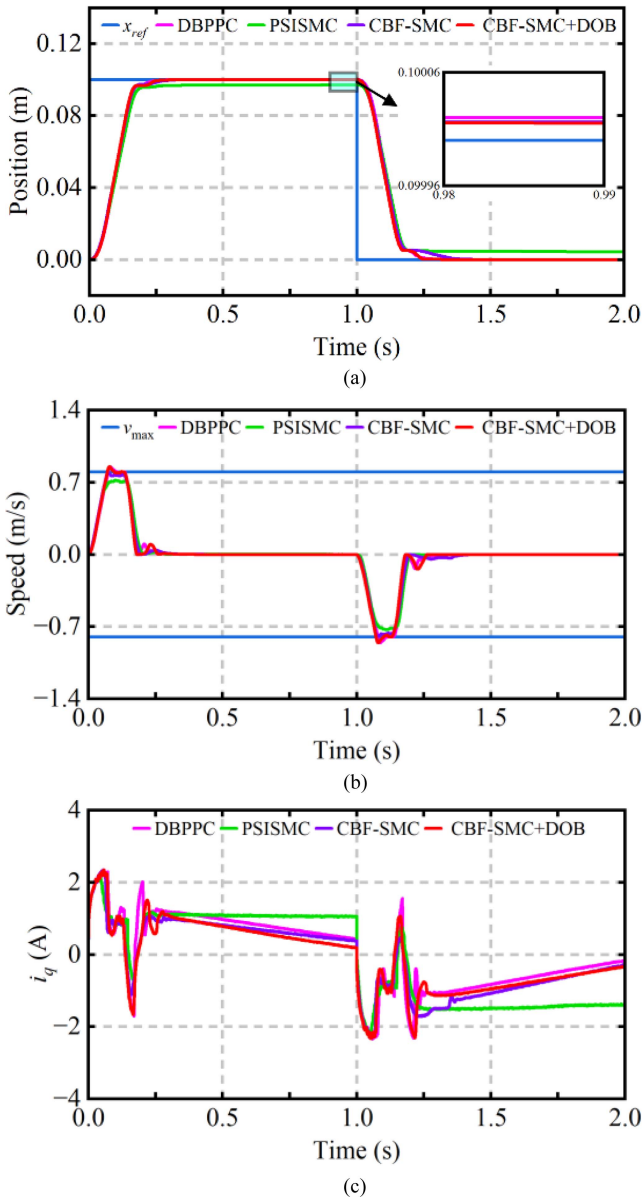

Fig. 9. Step response under speed constraint. (a) Position. (b) Speed. (c) q-axis current.

D. Parameter Variation Test

In order to investigate the impact of parameter changes on the performance of CBF-SMC and provide reference for parameter tuning, this part studied the dynamic performance and speed constraint capability of CBF-SMC with changes in parameters such as α, Δ, and τ_1, and conducted relevant experimental tests.

In order to study the effect of α variation on servo system, a sine reference position signal $x^* = 0.05\sin(2\pi t)$ is applied to the servo system of PMLSM. The maximum speed $v_{\max p}$ and $v_{\max n}$ are both set as 2m/s. In the test, the α values are changed to 0.3, 0.5, and 0.7, respectively. The sine response of CBF-SMC with α variation is shown in Fig. 11.

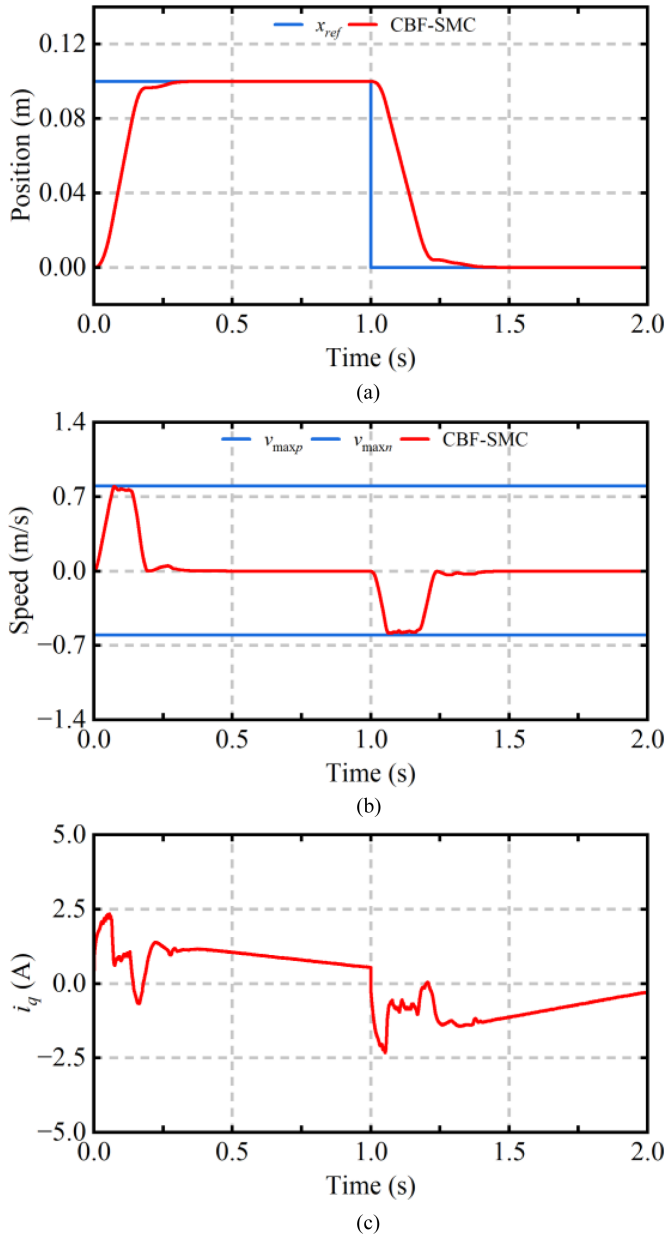

Fig. 10. Step response of CBF-SMC under asymmetric speed constraint. (a) Position. (b) Speed. (c) q-axis current.

Fig. 11 clearly shows the relationship between dynamic position error Δx_d and α. According to Fig. 11(a) and test data, the position time lag Δt_d under three different α are 0.0035 s, 0.0074 s, and 0.0188 s, respectively. The position dynamic error Δx_d under three different α are 0.0066746 m, 0.0106808 m and 0.0140048 m, respectively. Obviously, the increase in α will lead to a decrease in the dynamic performance of the method. Since α determines the power of the sliding mode reaching law, an increase in α is equivalent to a decrease in the controller gain, and the experimental results are consistent with this analysis.

In order to study the effect of Δ variation on servo system, a sine reference position signal $x^* = 0.05\sin(2\pi t)$ is applied

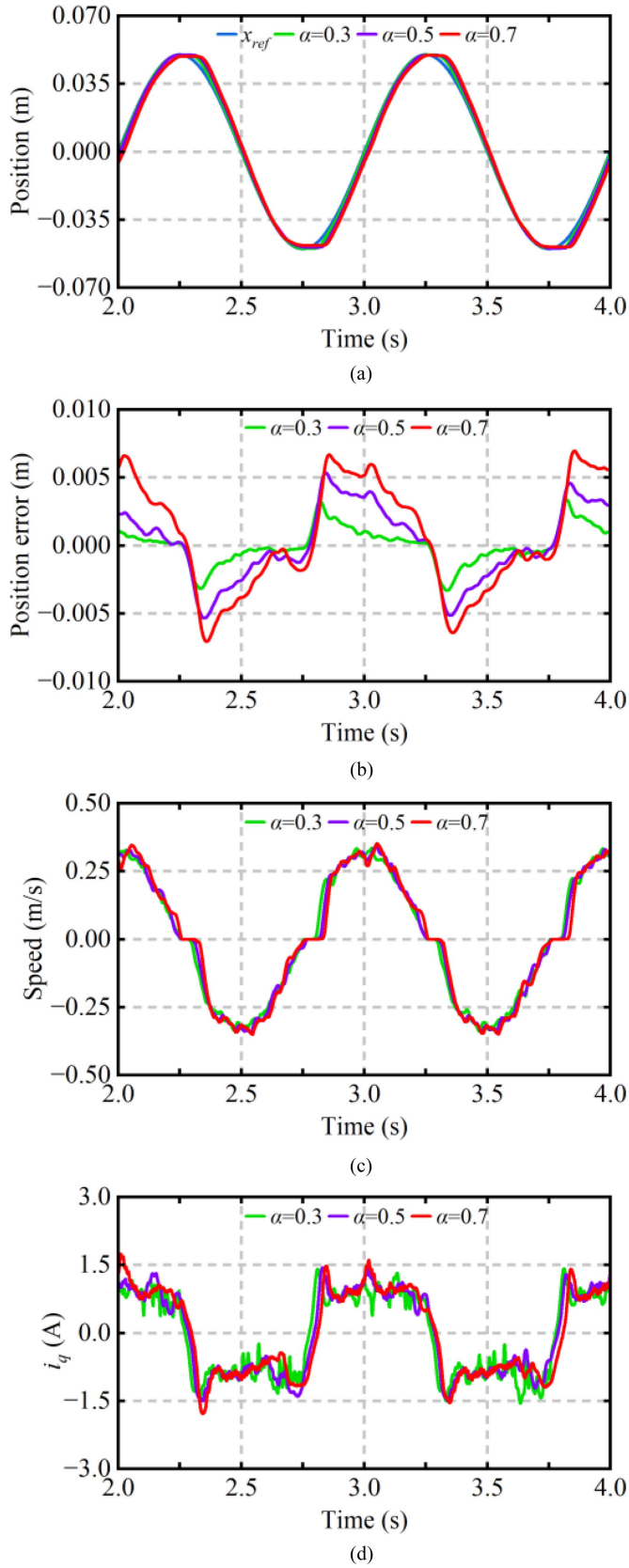

Fig. 11. Sine response of CBF-SMC with α variation. (a) Position. (b) Position error. (c) Speed. (d) q-axis current.

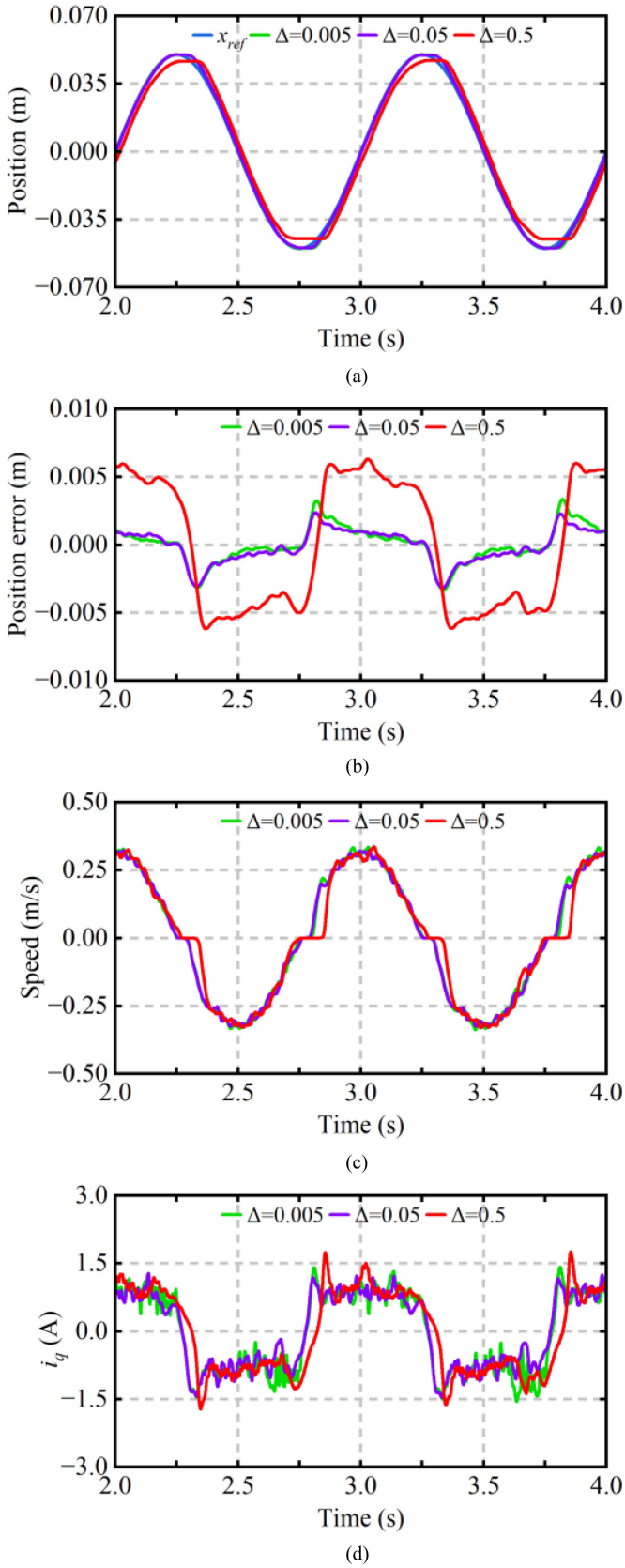

Fig. 12. Sine response of CBF-SMC with Δ variation. (a) Position. (b) Position error. (c) Speed. (d) q-axis current.

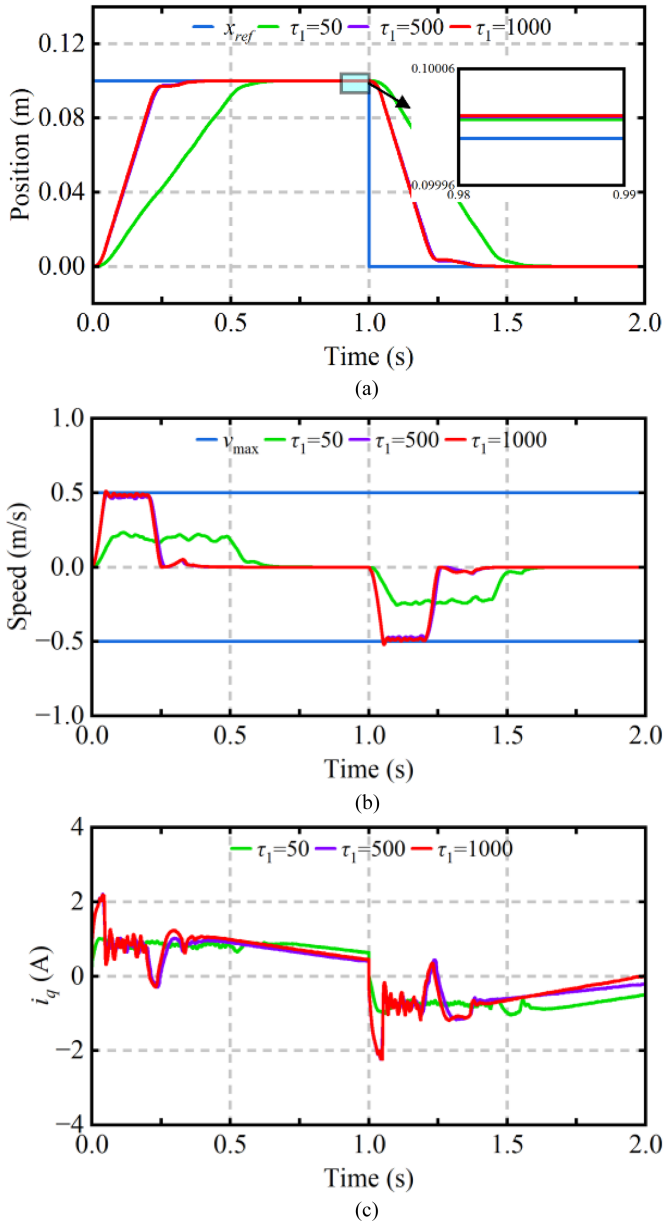

Fig. 13. Step response of CBF-SMC under speed constraint with τ_1 variation. (a) Position. (b) Speed. (c) q-axis current.

to the servo system of PMLSM. The maximum speed $v_{\max p}$ and $v_{\max n}$ are both set as 2m/s. In the test, the Δ values are changed to 0.005, 0.05, and 0.5, respectively. The sine response of CBF-SMC with Δ variation is shown in Fig. 12.

According to Fig. 12, Δt_d of different Δ are 0.0035 s, 0.0031 s, and 0.0188 s, respectively. Δx_d of different Δ are 0.0066746 m, 0.0055786 m, and 0.0125124 m, respectively. The experimental test results show that increasing Δ appropriately near zero is beneficial for alleviating the adverse effects of nonsmooth switching of the switching function and improving system performance. However, excessive increase in Δ is equivalent to an increase in the power term of the sliding mode reaching law, which will reduce the controller gain and decrease system performance.

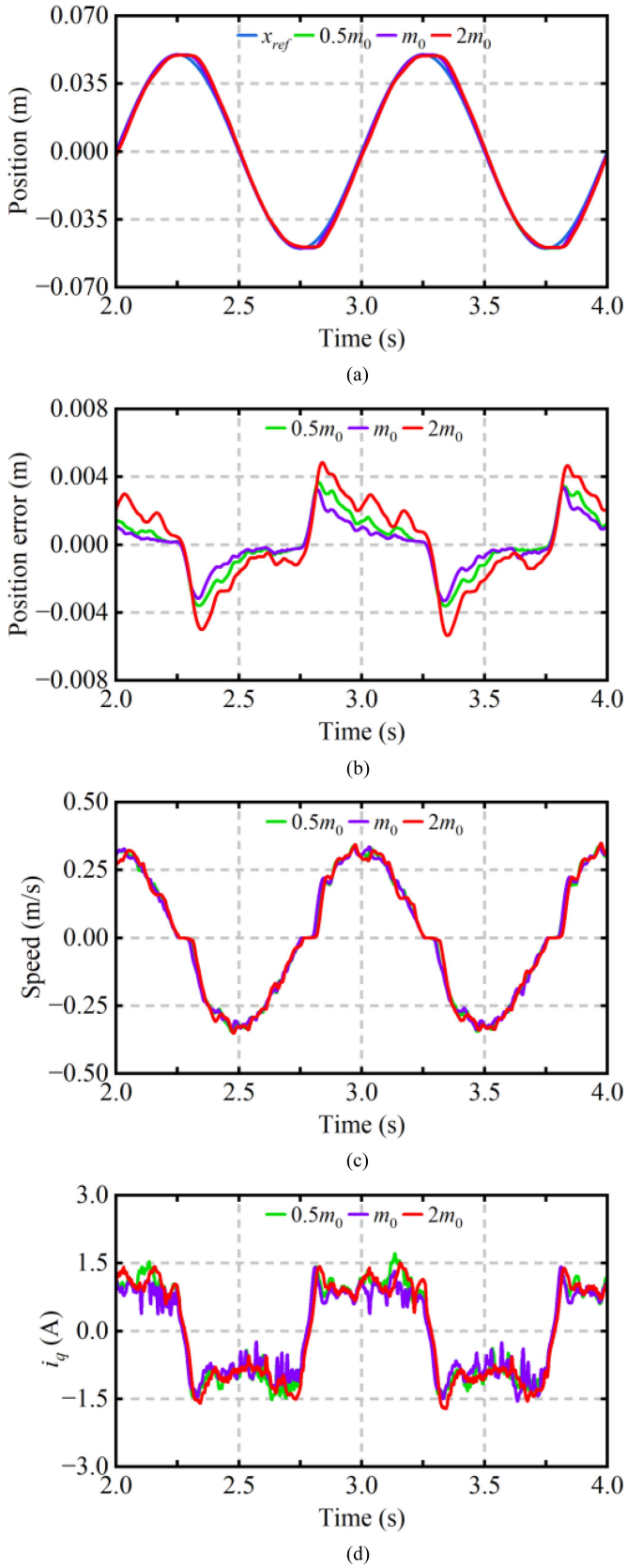

Fig. 14. Sine response of CBF-SMC method with m variation. (a) Position. (b) Position error. (c) Speed. (d) q-axis current.

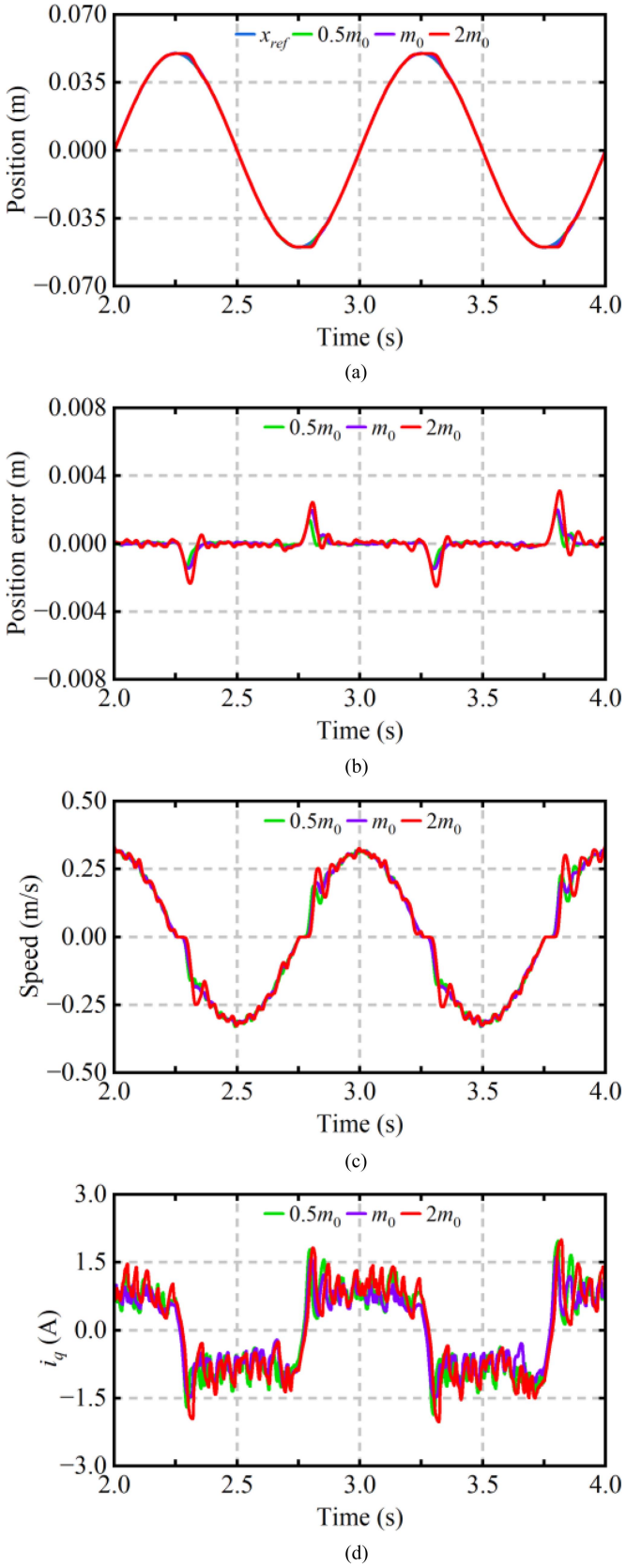

Fig. 15. Sine response of CBF-SMC + DOB method with m variation. (a) Position. (b) Position error. (c) Speed. (d) q-axis current.

In order to study the effect of τ_1 variation on speed constraint, a step reference position signal with 0.1 at 0 s and 0 at 1s is applied to the system. $v_{\max p}$ and $v_{\max n}$ are both set as 0.5 m/s. The step response under speed constraint of CBF-SMC with τ_1 variation is shown in Fig. 13.

According to the test results in Fig. 13, the larger τ_1 is, the closer the actual maximum speed is to the speed constraint, as previously stated in (20). In practical use, as a control gain at maximum speed, τ_1 should be increased as much as possible to fully utilize the speed constraint range without causing significant speed oscillations.

E. Robustness Test

Considering that there may be additional disturbances such as parameter changes and unmodeled dynamics in the control system, in order to verify the effectiveness of the proposed CBF-SMC in uncertain environments and the improvement of the robustness of the method by DOB, the effects of system parameter changes on the dynamic performance of the CBF-SMC method and CBF-SMC+DOB method are studied separately.

In the test, the PMLSM model parameter m is changed to 0.5 times and 2 times the m_0, respectively. A sine reference position signal $x^* = 0.05\sin(2\pi t)$ is applied to the servo system of PMLSM. The sine responses of CBF-SMC method and CBF-SMC+DOB method are shown in Figs. 14 and 15, respectively

According to Fig. 14 and experimental data, Δt_d of CBF-SMC method with m variation are 0.0047 s, 0.0035 s, and 0.0078 s, respectively. Δx_d of CBF-SMC method with m variation are 0.0072871 m, 0.0066746 m, and 0.0102000 m, respectively.

According to Fig. 15, Δt_d of CBF-SMC+DOB method with m variation are 0.0001 s, 0.0002 s, and 0.0005 s, respectively. Δx_d of CBF-SMC+DOB method with m variation are 0.0033924 m, 0.0034938 m, and 0.0056244 m, respectively. By analyzing two sets of experimental results, it can be found that parameter changes will have adverse effects on the performance of the method, and the integration of disturbance observer can enhance the robustness of the method to parameter changes.

V. Conclusion

In this article, a speed-constrained SMPC for PMLSM based on CBF has been proposed. By appropriately selecting the parameters of CBF, speed can be effectively constrained. In addition, a new sliding mode reaching law consisting of DPRL and a supertwisting-like integral term is proposed. The reaching law, when used in conjunction with CBF, can alleviate the contradiction between sliding mode chattering and convergence speed, as well as the low-speed crawling phenomenon in servo system of PMLSM. The BIBO stability of CBF-SMC is analyzed. Finally, experiment verified the superiority of the proposed method in terms of positioning and tracking performance, as well as the effectiveness of its speed constraint.

References

[1] D. Fu, X. Zhao, and J. Zhu, "A novel robust super-twisting nonsingular terminal sliding mode controller for permanent magnet linear synchronous motors," *IEEE Trans. Power Electron.*, vol. 37, no. 3, pp. 2936–2945, Mar. 2022.

[2] A. Wang, L. Li, and X. Huang, "Improved discrete-time resonant extended state observer based robust DPCC of winding-discontinuous-segmented PMLSM," *IEEE Trans. Ind. Electron.*, vol. 72, no. 6, pp. 5716–5727, Jun. 2025.

[3] L. Xiao, J. Zhang, H. Xie, and C. Hu, "A novel speed estimation algorithm for a permanent magnet linear synchronous motor using an extended kalman filter with multiple fading factors," *IEEE Trans. Magn.*, vol. 60, no. 11, Nov. 2024, Art. no. 8205205.

[4] K. Kang, M. Wang, J. Cui, C. Zhang, and L. Li, "Improved adaptive linear active disturbance rejection control for precise position control in permanent magnet linear synchronous motor," *IEEE Trans. Ind. Electron.*, vol. 72, no. 2, pp. 1795–1805, Feb. 2025.

[5] T. Wu et al., "A novel thermal analysis method for tubular PM linear motors based on transfer learning," *IEEE Trans. Transp. Electrific.*, vol. 11, no. 3, pp. 7379–7388, Jun. 2025.

[6] C. He, J. Hu, X. Ran, F. Wei, Y. Li, and Y. Zhu, "A simplified constrained predictive position control for PMSM drives with laguerre functions," *IEEE Trans. Ind. Electron.*, vol. 71, no. 12, pp. 15478–15487, Dec. 2024.

[7] A. K. Junejo et al., "Novel sliding mode reaching law based on DTC for linear induction machine applied to linear metro," *IEEE Trans. Transp. Electrific.*, vol. 10, no. 3, pp. 6460–6472, Sep. 2024.

[8] Y. Jiang, R. Wang, R. Ding, and Q. Ye, "Dual-loop model predictive control of permanent magnet linear synchronous motor for active suspension," *IEEE Trans. Energy Convers.*, vol. 40, no. 1, pp. 80–92, Mar. 2025.

[9] L. Wang, J. Zhao, Z. Yu, Z. Pan, and Z. Zheng, "High-precision position control of PMLSM using fast recursive terminal sliding mode with disturbance rejection ability," *IEEE Trans. Ind. Informat.*, vol. 20, no. 2, pp. 2577–2588, Feb. 2024.

[10] Y. Zhang, X. Huang, W. Yu, and J. Xu, "A general formulation of full-decoupled two-degree-of-freedom position controller for PMSLM based on ADRC," *IEEE Trans. Ind. Appl.*, early access, doi: 10.1109/TIA.2025.3587219.

[11] J. Yan, C. Wang, Z. Duan, L. Shan, and S. Chi, "Enhanced two-degree-of-freedom integrated position tracking control strategy for PMSM servo systems based on SMCFO-LADRC," *IEEE Trans. Transp. Electrific.*, vol. 11, no. 1, pp. 3931–3941, Feb. 2025.

[12] M. Zheng, Z. Zou, Q. Lu, Y. Li, and Y. Shen, "A simple modified deadbeat direct thrust control for permanent magnet linear synchronous machine considering parameter asymmetry," *IEEE Trans. Ind. Appl.*, vol. 59, no. 3, pp. 3163–3174, May/Jun. 2023.

[13] C. He, J. Hu, and Y. Li, "Predictive position control with system constraints for PMSM drives based on geometric optimization," *IEEE Trans. Ind. Electron.*, vol. 70, no. 8, pp. 7773–7782, Aug. 2023.

[14] J. Lin, W. Jiang, L. Zhou, J. Sun, and X. Song, "Improved model-free sliding mode control of linear motor based on time-varying gain model-assisted linear extended state observer," *IEEE Access*, vol. 12, pp. 20726–20733, 2024.

[15] L. Wang, J. Zhao, Z. Yu, Z. Pan, and Z. Zheng, "Robust and high-precision position control of PMLSM-driven feed servo system based on adaptive fast nonsingular terminal sliding mode," *IEEE Trans. Transp. Electrific.*, vol. 11, no. 1, pp. 4882–4894, Feb. 2025.

[16] H. Hou, X. Yu, L. Xu, K. Rsetam, and Z. Cao, "Finite-time continuous terminal sliding mode control of servo motor systems," *IEEE Trans. Ind. Electron.*, vol. 67, no. 7, pp. 5647–5656, Jul. 2020.

[17] X. He, X. Li, and S. Song, "Nonsingular terminal sliding-mode control of second-order systems subject to hybrid disturbances," *IEEE Trans. Circuits Syst. II Exp. Briefs*, vol. 69, no. 12, pp. 5019–5023, Dec. 2022.

[18] J. Wu, Y. Zhao, Y. Kong, Q. Liu, and L. Zhang, "Hierarchical nonsingular terminal sliding mode control with finite-time disturbance observer for PMSM speed regulation system," *IEEE Trans. Transp. Electrific.*, vol. 10, no. 3, pp. 4757–4765, Sep. 2024.

[19] S. Shi, X. Guo, S. Xu, H. Min, and L. Dai, "Recursive higher order nonsingular terminal sliding mode control with prescribed convergence time: Application to PMSM servo systems," *IEEE Trans. Automat. Sci. Eng.*, vol. 22, pp. 17955–17966, 2025.

[20] X. Guo, S. Huang, K. Lu, Y. Peng, H. Wang, and J. Yang, "A fast sliding mode speed controller for PMSM based on new compound reaching law with improved sliding mode observer," *IEEE Trans. Transp. Electrific.*, vol. 9, no. 2, pp. 2955–2968, Jun. 2023.

[21] X. Guo et al., "An improved integral sliding mode control for PMSM drives based on new variable rate reaching law with adaptive reduced-order PI observer," *IEEE Trans. Transp. Electrific.*, vol. 9, no. 3, pp. 4503–4516, Sep. 2023.

[22] S. Yin and X. Wang, "Super twisting control design for HSPMSG voltage stabilization based on disturbance observation compensation," *IEEE Trans. Energy Convers.*, vol. 38, no. 2, pp. 1387–1395, Jun. 2023.

[23] Q. Hou, S. Ding, X. Yu, and K. Mei, "A super-twisting-like fractional controller for SPMSM drive system," *IEEE Trans. Ind. Electron.*, vol. 69, no. 9, pp. 9376–9384, Sep. 2022.
[24] B. Tang, W. Lu, B. Yan, K. Lu, J. Feng, and L. Guo, "A novel position speed integrated sliding mode variable structure controller for position control of PMSM," *IEEE Trans. Ind. Electron.*, vol. 69, no. 12, pp. 12621–12631, Dec. 2022.
[25] Z. Yin, L. Gong, C. Du, J. Liu, and Y. Zhong, "Integrated position and speed loops under sliding-mode control optimized by differential evolution algorithm for PMSM drives," *IEEE Trans. Power Electron.*, vol. 34, no. 9, pp. 8994–9005, Sep. 2019.
[26] A. D. Ames, X. Xu, J. W. Grizzle, and P. Tabuada, "Control barrier function based quadratic programs for safety critical systems," *IEEE Trans. Automat. Control*, vol. 62, no. 8, pp. 3861–3876, Aug. 2017.
[27] K. Shao, J. Zheng, and M. Fu, "Review on the developments of sliding function and adaptive gain in sliding mode control," *J. Automat. Intell.*, early access, doi: 10.1016/j.jai.2025.06.001.
[28] K. Shao, J. Zheng, R. Tang, X. Li, Z. Man, and B. Liang, "Barrier function based adaptive sliding mode control for uncertain systems with input saturation," *IEEE/ASME Trans. Mechatron.*, vol. 27, no. 6, pp. 4258–4268, Dec. 2022.
[29] L. Chen et al., "Sensorless fixed-time sliding mode control of PMSM based on barrier function adaptive super-twisting observer," *IEEE Trans. Power Electron.*, vol. 39, no. 3, pp. 3037–3051, Mar. 2024.
[30] J. Gu, S. You, W. Kim, and J. Moon, "Fuzzy event-triggered super twisting sliding mode control for position tracking of permanent magnet synchronous motors under unknown disturbances," *IEEE Trans. Ind. Informat.*, vol. 19, no. 9, pp. 9843–9854, Sep. 2023.
[31] J. Hu, C. He, and Y. Li, "A novel predictive position control with current and speed limits for PMSM drives based on weighting factors elimination," *IEEE Trans. Ind. Electron.*, vol. 69, no. 12, pp. 12458–12468, Dec. 2022.

Zekun Wang (Student Member, IEEE) received the B.E. degree in electrical engineering in 2022 from the Harbin Institute of Technology, Harbin, China, where he is currently working toward the Ph.D. degree in electrical engineering.

His current research interests include the permanent magnet linear synchronous motor control and servo control.

Chun He received the M.S. and Ph. D. degrees in electrical engineering from the Harbin Institute of Technology, Harbin, China, in 2019 and 2023, respectively.

He is currently a Postdoctoral Researches in electrical engineering with Harbin Institute of Technology. His current research interests include the permanent magnet synchronous motor control and model predictive control.

Yong Li received the Ph.D. degree in electrical engineering from the Harbin Institute of Technology, Harbin, China, in 1988.

He is currently a Professor with the Department of Electrical Engineering, Harbin Institute of Technology. His research interests include PMSMs, special motors.

Mingqiao Wang (Member, IEEE) received the B.S. and Ph.D. degree in electrical engineering from Harbin Institute of Technology, Harbin, China, in 2016 and 2021, respectively.

Since 2022, he has been with Harbin Institute of Technology, where he has been an Associate Research Fellow since 2025. He is the author or coauthor of 37 published refereed technical papers. He is the holder of 19 Chinese invention patents. His current research interests include design and control of variable flux machines, and the intelligent computing of electric machine system.

Chenxiao Jiu received the B.S. degree in electrical engineering from Harbin Institute of Technology, Harbin, China, in 2008.

He is currently with the Xi'an Flight Automatic Control Research Institute, Xi'an, China. His research interests include high-performance aeronautic servo motors design, modeling, and simulation.